Local structure, transport, and rare-earth magnetism in the ferrimagnetic perovskite $Gd_{0.67}Ca_{0.33}MnO_3$

G. Jeffrey Snyder
Department of Applied Physics, Stanford University, Stanford, California 94305-4090

C. H. Booth and F. Bridges
Department of Physics, University of California Santa Cruz, Santa Cruz, California 95064

Ron Hiskes and Steve DiCarolis
Hewlett-Packard, Palo Alto, California 94303-0867

M. R. Beasley and T. H. Geballe
Department of Applied Physics, Stanford University, Stanford, California 94305-4090

(Received 3 September 1996; revised manuscript received 24 October 1996)

Bulk, single crystal, and metal-organic chemical-vapor deposition thin-film samples of $Gd_{0.67}Ca_{0.33}MnO_3$ were prepared and examined for their electrical, magnetic, and structural properties. $Gd_{0.67}Ca_{0.33}MnO_3$ is ferrimagnetic with a transition temperature between 50 and 80 K and a compensation temperature of about 15 K. A molecular field model with a ferromagnetic manganese sublattice antiparallel to the gadolinium sublattice qualitatively explains the magnetism data. A large high-field susceptibility is observed at 5 K, suggesting a sublattice rotation. The resistivity and the magnetoresistance show no anomaly near the ferrimagnetic transition. There is no noticeable change in the structure, as seen from the x-ray-absorption fine structure between 40 and 69 K, indicating that there is no structural discontinuity across the paramagnetic insulator to ferromagnetic insulator phase boundary. The resistivity of $Gd_{0.67}Ca_{0.33}MnO_3$ is consistent with small polaron hopping at high temperatures (up to 1100 K), and possibly by a different mechanism at low temperatures.
[S0163-1829(97)01010-2]

I. INTRODUCTION

The mixed valent $R_{1-x}A_xMnO_3$ perovskite manganates, where R and A are rare-earth and alkaline-earth elements, respectively, have received much attention due to their unusual electronic and magnetic properties. Most of these compounds are either metals or highly conducting semiconductors. For this reason, and because they are very stable under oxidizing conditions at high temperature, these perovskites have been used for the cathode material in solid-oxide fuel cells.[1] Some of these materials, particularly the lanthanum-containing compounds, show a paramagnetic-semiconductor to ferromagnetic-metal transition upon cooling. This peculiarity has spawned the theory of double exchange to explain such a transition.[2] More recently, very large magnetoresistances have been found in materials which show this metal-insulator transition (see, for example, Ref. 3). It has been proposed that a structural transition accompanies the ferromagnetic transition, and the relative importance of each in promoting the metal-insulator transition is of particular interest.[4]

In order to examine the nature of this metal-insulator transition, we have chosen to study $Gd_{0.67}Ca_{0.33}MnO_3$. The composition $x=\frac{1}{3}$ was chosen because this doping concentration should maximize the double exchange effect as seen in the lanthanum compounds.[5] Due to the small size of the Gd^{3+} ion, $Gd_{0.67}Ca_{0.33}MnO_3$ should be in the region of the $x=\frac{1}{3}$ phase diagram where there is no transition to a metallic state, but to a ferromagnetic insulating state around 50 K.[6] The ferromagnetic nature of this low-temperature state has recently been questioned due to evidence of a spin-glass behavior with no long-range ferromagnetic order in $(Tb_xLa_{1-x})_{0.67}Ca_{0.33}MnO_3$.[7] The x-ray-absorption fine-structure (XAFS) technique can detect small variations of the average local environment about a particular atomic species, making it ideal for studying subtle structural phase transitions associated with such metal-insulator or magnetic transitions. The Mn K edge (6.54 keV) and Gd L_{III} edge (7.25 keV) are well enough separated that there is little interference of the Mn and Gd XAFS.

In this study, we have found that the rare-earth moments in $Gd_{0.67}Ca_{0.33}MnO_3$ order antiparallel to the manganese, giving rise to ferrimagnetism. Furthermore, we find that not only does this material remain insulating when it becomes magnetically ordered, but we also find that no structural difference exists between the ferrimagnetic and paramagnetic state. This is consistent with models that require a structural change, as well as the ferromagnetic ordering of the manganese atoms, to explain the metal-insulator transition and the large magnetoresistance that accompanies it.

II. EXPERIMENT

A. Sample preparation

Three types of samples were prepared: polycrystalline pellets, float-zone crystals, and thin films. Polycrystalline samples of $Gd_{0.67}Ca_{0.33}MnO_3$ were made using standard ceramic synthesis techniques. Gd_2O_3, $CaCO_3$, and MnO were

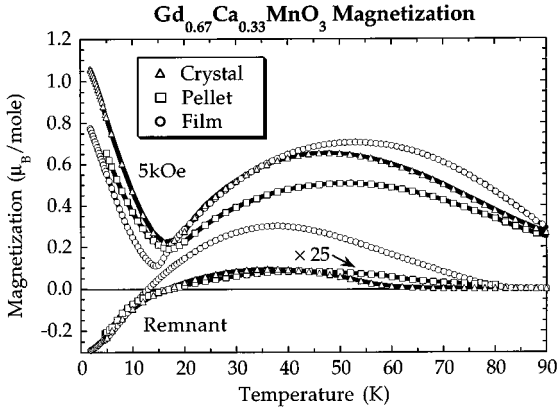

FIG. 1. Low-temperature magnetization of $Gd_{0.67}Ca_{0.33}MnO_3$ measured in a 5-kOe field and zero field after cooling in a large field (remnant).

repeatedly reacted in air at 1250 °C for several days. Pellets were cold pressed and sintered under the same conditions. Powder x-ray diffraction showed single phase orthorhombic perovskite (*Pnma*; $a=5.52$ Å, $b=7.50$ Å, $c=5.34$ Å) as reported previously.[1]

From this material, float-zone crystals were grown using a CO_2 laser heated pedestal growth system.[8,9] The approximately 1-mm-diameter crystals were grown at about 1 cm/h.

The solid source metal-organic chemical-vapor deposition reactor used to grow the films in this study has been described previously.[10] The 2,2,6,6-tetramethyl-3,5-heptanedionato (TMHD) organometallic complexes used for Gd, Ca, and Mn were, respectively, tris(TMHD) gadolinium, bis(TMHD) calcium, and tris(TMHD) manganese $LaAlO_3$ substrate temperatures of 600 °C were used in an oxygen partial pressure of 3–4 torr. 1500-Å-thick films were grown at approximately 45 Å/min. The films were then annealed in flowing oxygen at 950 °C for several hours and cooled slowly (~20 °C/h) to room temperature. The composition of the source material was based on our experience with lanthanum-based compounds.[3]

B. Magnetization measurements

A Quantum Design $MPMS_2$ superconducting quantum interference device magnetometer was used for magnetization

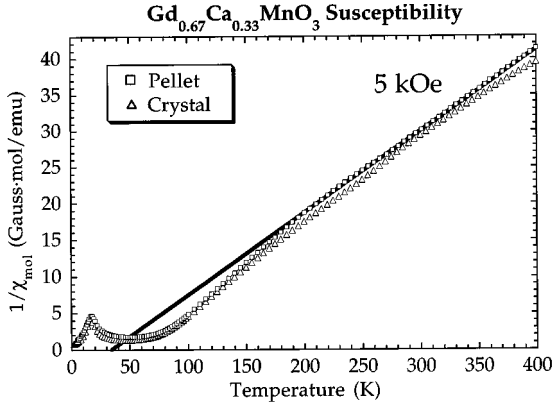

FIG. 2. Inverse magnetic susceptibility of bulk $Gd_{0.67}Ca_{0.33}MnO_3$. Solid line is the high-temperature fit to $\chi=\mu_{\text{eff}}^2/[8(T-\Theta)]$ described in the text.

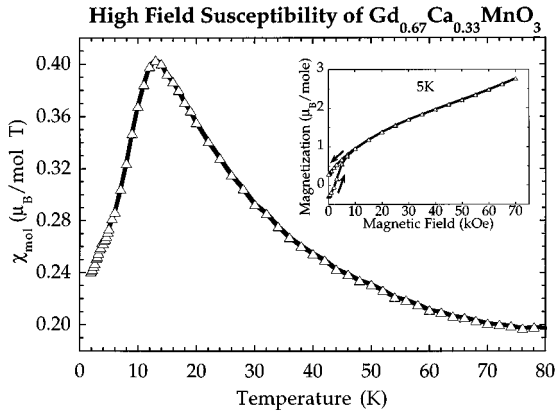

FIG. 3. Low-temperature and high-field magnetic susceptibility, $\chi=[M(60\text{ kOe})-M(40\text{ kOe})]/20$ kOe, of $Gd_{0.67}Ca_{0.33}MnO_3$ crystal. Inset, hysteresis loop at 5 K.

M and resistivity ρ measurements at temperatures T from 2 to 400 K and magnetic fields H up to 6 T. Measured data of thin films contained contributions from the film and the $LaAlO_3$ substrate, which is diamagnetic with a small contribution from a paramagnetic impurity.[3] The ferrimagnetic transition temperature T_c was estimated by three methods, all of which give the same result (±0.2 K) in the molecular field model.[11] The remnant T_c is the temperature where the bulk of the magnetization, in zero or small field, vanishes. The inflection T_c is the temperature of the inflection point in the M vs T curve. The Arrott T_c is the temperature where the M^2 vs H/M curve extrapolates to the origin.[12]

C. Electronic transport measurements

Four leads were attached with indium for measurements less than 400 K or polyimide-based silver epoxy for above 400 K (in air) either in the van der Pauw[13] or conventional configuration. dc currents were chosen well within the Ohmic regime. Offset voltages were subtracted by reversing the current. Voltages were measured at several slightly (up to 20%) different currents to calculate the precision. For resistances greater than $10^6\Omega$ or $T<100$ K, two point resistance measurements were made using an electrometer.

D. XAFS measurements

X-ray absorption spectra were collected in transmission mode on beam line 4-3 at the Stanford Synchrotron Radia-

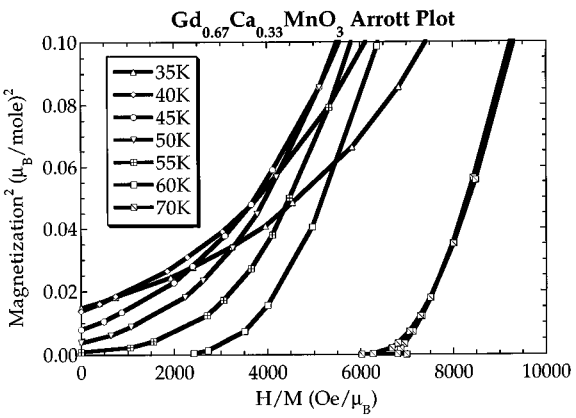

FIG. 4. Arrott plot of polycrystalline $Gd_{0.67}Ca_{0.33}MnO_3$ pellet.

TABLE I. Transition temperatures for $Gd_{0.67}Ca_{0.33}MnO_3$.

	T_{Comp} (K)	Arrott T_c (K)	Remnant T_c (K)	Inflection T_c (K)
Polycrystalline pellet	17	52	60	80
Single crystal	17	56	62	78
Thin film	13	70	81	88

tion Laboratory using powder samples (grain size less than 30 μm. The sample temperature was regulated using an Oxford helium cryostat system within 0.1 K (absolute temperature may be as much as 2 K warmer). Data for this experiment were collected above and below T_c, at $T=69$ K and 40 K. Data reduction and analysis followed standard procedures reported previously.[14]

III. RESULTS

A. Magnetism

The polycrystalline pellets, crystals, and thin films all display a ferromagnetic transition and a compensation temperature (Fig. 1), which is characteristic of ferrimagnets. Both bulk materials, polycrystalline pellet and float-zone crystal, have very similar magnetic properties, while the film is slightly different. The molar magnetic susceptibility χ (Fig. 2) above 200 K can be fit to the Curie-Weiss law: $\chi=\mu_{\rm eff}^2/[8\ (T-\Theta)]$ with $\mu_{\rm eff}^2=71\ \mu_B^2$ and $\Theta=34$ K. The difference in the susceptibility of the crystal compared to that of the pellet at high temperatures may not be significant. The hysteresis loop at 5 K (Fig. 3) shows an additional high-field paramagnetic response not expected for a mean-field ferrimagnet. The experimental values of T_c are summarized in Table I. An example of the nonlinear M^2 vs H/M Arrott plot is given in Fig. 4. The calculated magnetization and inverse susceptibility for the molecular field model described below is shown in Fig. 5.

B. Electronic transport

The resistivity can be well approximated by $R_hT\exp(E_a/k_BT)$ (Fig. 6), predicted by small polaron hopping conductivity.[15,16] Below about 150 K (Fig. 7), the resistivity is somewhat better described by $R_0\exp(T_0/T)^{1/4}$, which is commonly attributed to variable range hopping.[17] The quantitative aspects of the fits is discussed below. The thin-film and crystal samples show no transition to a metallic state down to 5 K. No extraordinary magnetoresistance was observed in the entire temperature range. The magnetoresistance at 200 and 300 K is a few percent in a 70-kOe field, and approximately proportional to H^2 (Fig. 7). Reliable resistivity data could be measured on the crystal sample down to 40 K. No discontinuity in the resistivity was found near T_c.

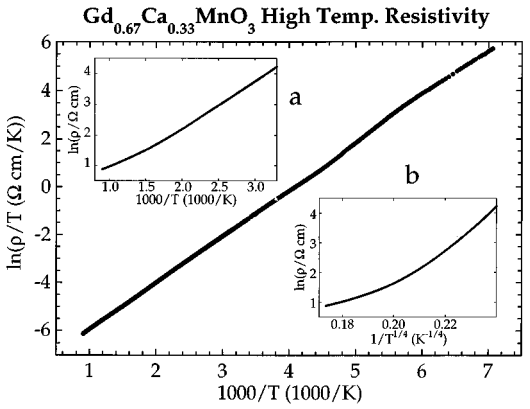

FIG. 6. High-temperature resistivity during heating and cooling a $Gd_{0.67}Ca_{0.33}MnO_3$ film, $\ln(\rho/T)$ vs $1/T$. Inset a, comparison with $\ln(\rho)$ vs $1/T$. Inset b, comparison with $\ln(\rho)$ vs $1/T^{1/4}$.

C. XAFS

The primary quantity in XAFS data analyses is $\chi(k)=[\mu(k)-\mu_0(k)]/\mu_0(k)$, where k is the ejected photoelectron wave vector, $\mu(k)$ is the total absorption due to the absorbing atomic species, and $\mu_0(k)$ is the portion of $\mu(k)$ that does not include the photoelectron backscattering off neighboring atoms. This backscattering causes an interference at the absorbing atom which is manifest as oscillations in $\chi(k)$. A Fourier transform of $k\chi(k)$ thus produces peaks

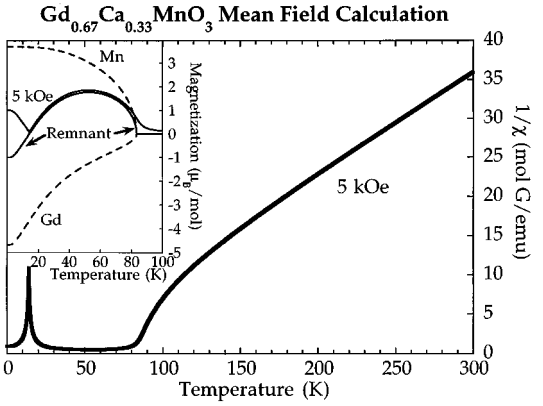

FIG. 5. Magnetization and inverse magnetic susceptibility calculated for $Gd_{0.67}Ca_{0.33}MnO_3$ using the simplified mean-field theory described in the text and $T_c=83$ K, $T_{Comp}=17$ K. The contribution to the magnetization of each sublattice is shown in dashed lines.

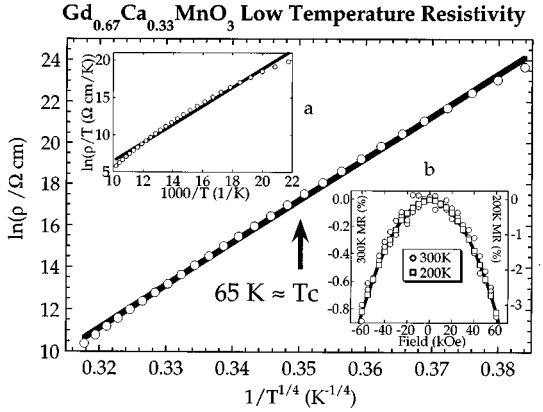

FIG. 7. Low-temperature resistivity of $Gd_{0.67}Ca_{0.33}MnO_3$ crystal, $\ln(\rho)$ vs $1/T^{1/4}$. Inset a, comparison with $\ln(\rho/T)$ vs $1/T$. Solid lines show linear best fit to the data shown. Inset b, magnetoresistance of a film at 200 and 300 K; solid line is the quadratic fit.

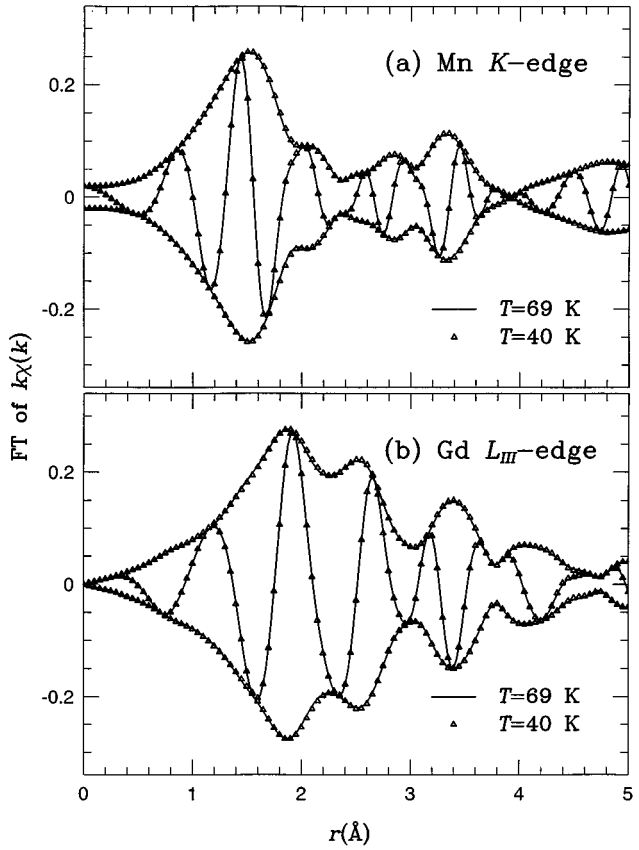

FIG. 8. Fourier transform of $k\chi(k)$ from (a) Mn K-edge and (b) Gd L_{III}-edge data on $Gd_{0.67}Ca_{0.33}MnO_3$. The solid lines are data collected at $T=69$ K, while the triangles (△) are data collected at $T=40$ K. Agreement between data above and below T_c is well within the errors of the experiment. Transform ranges for the Gd edge data are from 3.5–12.5 $Å^{-1}$ and Gaussian broadened by 0.3 $Å^{-1}$. Transform ranges for the Mn edge data are from 3.2–12.5 $Å^{-1}$ and Gaussian broadened by 0.3 $Å^{-1}$.

that correspond to the distribution of atoms around the absorbing atom. Figure 8 shows these Fourier transforms.

The agreement between the data above and below T_c is very good and places limits on any atom-position changes around either the Gd or Mn atoms within 0.005 Å, and changes in the Debye-Waller broadening factor to 0.002 Å.

IV. DISCUSSION

$Gd_{0.67}Ca_{0.33}MnO_3$ displays the properties of a ferrimagnet, much like the garnet ferrite $Gd_3Fe_5O_{12}$.[18] At about 60 K, the transition metal spins order, dominating the magnetization. As the temperature is lowered, the opposing magnetization of the weaker coupled rare-earth ions increases, since they behave almost as though they were free paramagnetic spins reacting to an internal field. Figure 3 is essentially the magnetic susceptibility of these rare-earth moments, showing an approximate $\chi \propto 1/(T+T_{\mathrm{Comp}})$ behavior until the Gd^{3+} moments effectively order antiferromagnetically with respect to the manganese moments below T_{Comp}. At the compensation temperature T_{Comp}, the rare-earth and transition metal sublattice magnetizations exactly cancel (in zero field). Below T_{Comp}, the magnetization of the rare-earth ions, which have larger spins, dominates. This is best seen in zero-field remnant data which shows the magnetization changing sign at T_{Comp}. The change in sign of the zero-field magnetization is characteristic of a ferrimagnet and not that of a spin glass. In the presence of magnetic fields greater than the coercive field, the stronger sublattice flips to align parallel with the field, giving the minimum in M at T_{Comp} as seen the 5-kOe data.

Due to the stronger $3d$ exchange interaction compared to that of the $4f$, we expect the Mn-Mn coupling to be stronger than the Mn-Gd, and the Gd-Gd interaction to be negligible. Since the observed Curie temperature is about that expected from the trend found in the manganese ferromagnetic ordering temperature as a function of the average of the R and A atom size in $R_{0.7}A_{0.3}MnO_3$.[6] If we assume for now that the Mn-Mn interaction in $Gd_{0.67}Ca_{0.33}MnO_3$ is ferromagnetic, the ferrimagnetism must then arise from a weaker, antiferromagnetic Mn-Gd interaction. Thus, unlike the ferrites, where the dominant interaction is antiferromagnetic between the two transition-metal sublattices, the strongest magnetic coupling in $Gd_{0.67}Ca_{0.33}MnO_3$ is ferromagnetic, much like that found in the rare-earth cobaltites, e.g., $GdCo_5$.[19]

The above description of the magnetization can be bolstered using a simple molecular or mean field model.[11] Assuming that all atoms on each sublattice (Mn or Gd) feel the same mean field, there are only two unknown mean-field coefficients due to the Mn-Mn and Mn-Gd interactions. These two coefficients are easily determined, since they are nearly proportional to T_c and T_{Comp}, respectively. This molecular field model (Fig. 5) reproduces the qualitative features described above.

The discrepancies in the salient features discussed below may result from the simplifications of the model, and the assumptions behind it. The evidence concerning the magnetic structure of the manganese in the ferromagnetic insulator phase points to a canted antiferromagnetic structure rather than a simple ferromagnet. The magnetic structure of $Pr_{0.67}Ca_{0.33}MnO_3$, which is on the boundary between ferromagnetic-insulator and ferromagnetic-metal low-temperature phases,[6] has been extensively studied. Neutron diffraction shows $Pr_{0.67}Ca_{0.33}MnO_3$ to have a charge-ordered, canted-antiferromagnetic structure in the low-temperature phase with ferromagnetic moment about half of the total expected moment.[20,21] A compound clearly in the ferromagnetic-insulator part of the tolerance-factor phase diagram, much closer to $Gd_{0.67}Ca_{0.33}MnO_3$ than $Pr_{0.67}Ca_{0.33}MnO_3$, is $La_{0.2}Y_{0.5}Ca_{0.3}MnO_3$. This compound appears to be ferromagnetic with about half the expected ferromagnetic moment,[6] which could be explained by a canted antiferromagnetic state similar to that found in $Pr_{0.67}Ca_{0.33}MnO_3$. Thus, one should expect the ferromagnetic moment of the Mn ions in $Gd_{0.67}Ca_{0.33}MnO_3$ to be half that predicted in the above molecular field model. If the Gd moments are also canted to the same degree, then the predicted magnetization will be qualitatively the same for the uncanted case (Fig. 5), only half the magnitude; namely, there will still be a compensation temperature.

The model is further limited by the obvious simplifications: not only are there two distinct types of Mn atoms (Mn^{3+} and Mn^{4+}), but there are numerous possible configurations for the number and type of near neighbors due to the

randomness on the Mn and Gd/Ca sites. The discrepancy among the various values of T_c determined by the three methods mentioned is an example of non-mean-field ferromagnetic behavior. Such atomic disorder can result in a spin glass, and indeed a spin-glass insulating low-temperature phase was found in $(Tb_xLa_{1-x})_{0.67}Ca_{0.33}MnO_3$ in place of the ferromagnetic insulator state. The compound $Tb_{0.67}Ca_{0.33}MnO_3$ should be in the same region of the tolerance-factor-phase diagram as $Gd_{0.67}Ca_{0.33}MnO_3$ and $La_{0.2}Y_{0.5}Ca_{0.3}MnO_3$. The Tb compound is apparently a pure spin glass with no long-range magnetic order.[7] The question of the existence or nonexistence of spin-glass behavior in $Gd_{0.67}Ca_{0.33}MnO_3$ is beyond the scope of this investigation. However, it is clear that $Gd_{0.67}Ca_{0.33}MnO_3$ has long-range magnetic order. The distinction is most obvious in the Arrott plot (Fig. 4), which shows that $Gd_{0.67}Ca_{0.33}MnO_3$ has a nonzero magnetization when $H=0$ below T_c, while $(Tb_{0.33}La_{0.67})_{0.67}Ca_{0.33}MnO_3$ does not.[7] The other striking feature of $Gd_{0.67}Ca_{0.33}MnO_3$ is the existence of a compensation point, which, to our knowledge, cannot be explained by a spin-glass magnetic system.

The saturation magnetization per mole of $Gd_{0.67}Ca_{0.33}MnO_3$ expected from the Gd^{3+} $s=\frac{7}{2}$, $l=0$ is $\mu=(0.67\times2\times7/2)\ \mu_B=4.67\ \mu_B$, while high-spin manganese gives spin only (orbital contribution quenched) $\mu=gs\mu_B$, $g=2$ so $\mu=2\ \mu_B[0.67\times2$ (from Mn^{3+})$+0.33\times\frac{3}{2}$ (from Mn^{4+})$]=3.67\ \mu_B$. The simple two sublattice Gd and Mn ferrimagnetism described above predicts a zero-temperature saturation magnetization of $4.67\ \mu_B-3.67\ \mu_B=1.00\ \mu_B$ (if there is any canting of the sublattices, such as that in $Pr_{0.67}Ca_{0.33}MnO_3$,[20] a smaller moment is predicted). This is roughly what is observed. The mean-field calculation predicts a constant moment for $T<5$ K, while the data show an almost linear increase in M for $2<T<5$ K. Also, the peak in the magnetization, observed at about 50 K in the 5-kOe data is less than the $1.9\ \mu_B$ predicted in the mean-field calculation.

The large field-dependent magnetization seen at 5 K is not predicted in the simple mean-field calculation. It is not uncommon, however, to observe such a field-induced increase of the magnetization in canted ferromagnetic or ferrimagnetic systems,[22,23] and it is used as evidence of the ferrimagnetic sublattices canting away from antiparallel.[24] The magnetic field affects the canting angle, which results in the magnetization increasing nearly linearly with field, even at $T=0$ K.[22] If this large susceptibility were due to a second phase with free paramagnetic spins, then this phase would have to contain at least half of the available spins and have a $1/T$ temperature dependence for all T. This is not seen in Fig. 3. Instead, the high-field susceptibility maximizes near $T_{\rm Comp}$ (Fig. 3), which is typical of an antiferromagnet with $T_N\approx T_{\rm Comp}$. This is predicted in the mean-field calculation for a ferrimagnet.[11]

Susceptibility data above 200 K fit to the Curie-Weiss law with $\Theta=34$ K and $\mu_{\rm eff}^2=71\ \mu_B^2$. For quantum mechanical spins $\mu_{\rm eff}^2$ per mole is expected to be $63\ \mu_B^2$: $2^2\mu_B^2(0.67\times\frac{4}{2}\times\frac{6}{2})=16\ \mu_B^2$ from Mn^{3+}; $2^2\mu_B^2(0.33\times\frac{3}{2}\times\frac{5}{2})=5\ \mu_B^2$ from Mn^{4+}; $2^2\mu_B^2(0.67\times\frac{7}{2}\times\frac{9}{2})=42\ \mu_B^2$ from Gd^{3+}. This extra moment, which is also observed in $La_{0.67}Ca_{0.33}MnO_3$,[3] may be due to the orbital contribution in the manganese ions. Since the two sublattices have different coupling energies, the susceptibility above T_c will not obey a simple Curie-Weiss law even in the mean-field approximation (Fig. 5). The simple mean-field model of the above ferrimagnetism requires $T_c/\Theta>3$.[11] This is clearly not the case for the measured parameters. Alternatively, the addition of a Pauli-like susceptibility χ_0 to the fit, $\chi=\chi_0+\mu_{\rm eff}^2/[8(T-\Theta)]$, will reduce the contribution from $\mu_{\rm eff}$. For example, an equally good fit to the data can be found with $\mu_{\rm eff}^2=63\ \mu_B^2$, $\chi_0=7.7\times10^{-6}$ emu G^{-1} g^{-1}, and $\Theta=50$ K.

Since Gd^{3+} has the largest spin of the rare-earth elements, it should have the highest ordering temperature. If the relevant exchange interaction is due to spin-spin coupling of the rare-earth and manganese atoms, then the strength of this interaction will be proportional to the spin S of the rare-earth ion. From this relation, we can estimate the ordering temperature of the rare-earth moments in related compounds to be about 7 K for $Nd_{0.67}Ca_{0.33}MnO_3$ and 5 K for $Pr_{0.67}Ca_{0.33}MnO_3$. This should result in a decrease in M at low T. This appears at temperatures lower than these estimates, if at all,[25,26] perhaps indicating an interaction strength proportional to S^2, the square of the rare-earth spin, or simply that these moments do not order antiparallel to the manganese moments.[27]

The electrical resistivity of $Gd_{0.67}Ca_{0.33}MnO_3$ is consistent with adiabatic small polaron hopping conductivity $R_hT\exp(E_a/k_BT)$,[15,28] $R_h=2k_B/3ne^2a^2\nu$, particularly at high temperatures. Here, k_B is Boltzmann's constant, e is the electronic charge, n is the number density of charge carriers—about 0.7 carrier per Mn—a is the site-to-site hopping distance, and ν is the longitudinal-optical phonon frequency. This behavior has also been observed in the La-containing compound.[3,16] Resistivity data are often displayed on an Arrhenius plot [$\ln(\rho)$ vs $1/T$], which will give a straight line for a band-gap semiconductor,[1,29] providing the mobility is not temperature dependent. The slightly different temperature dependence of the data provides the significant nonlinearity in such a fit (Fig. 6). We infer a polaron hopping activation energy E_a of 1940 K, and an attempt frequency of 8×10^{13} s^{-1}. The small polaron mechanism implies that unlike a band-gap semiconductor, the highly temperature-dependent quantity is the mobility, not the carrier concentration. A high, temperature-independent carrier concentration is consistent with Hall effect measurements on $La_{0.67}Ca_{0.33}MnO_3$.[3,30]

The resistivity of the manganites has also been attributed to variable-range hopping due to Anderson localization.[31] At temperatures less than 150 K, this picture produces a somewhat better fit to our data (Fig. 7), but is clearly inferior to the polaron model at high temperatures (Fig. 6). The fit to $R_0\exp(T_0/T)^{1/4}$ gives $T_0=1.7\times10^9$ K. In the theory of variable range hopping,[32,33] $k_BT_0\approx21/[\zeta^3N(E_F)]$ where ζ is the decay length of the localized wave function, and $N(E_F)$ is the density of localized states at the Fermi level. For $\zeta\approx a=3.9$ Å, the distance between neighboring Mn atoms, this implies $N(E_F)\approx2.4\times10^{18}$ eV^{-1} cm^{-3}, which is typical for disorder semiconductors, but about 1500 times less than the density of states found in the specific heat of manganites which become metallic at low temperatures (≈5 mJ mol^{-1} K^{-2}).[34]

Unlike the colossal magnetoresistance manganites, $Gd_{0.67}Ca_{0.33}MnO_3$ does not have a metal-insulator transition or a large magnetoresistance near the Curie temperature. The

negative magnetoresistance is only of order 1% in large fields and is proportional to H^2 (or M^2, since it scales with χ^2) like that observed in $La_{0.67}Ca_{0.33}MnO_3$ in the paramagnetic state.[30] Thus, $Gd_{0.67}Ca_{0.33}MnO_3$ is clearly in the class of $\frac{1}{3}$ doped manganites which, due to the small size of Gd^{3+},[6] change from paramagnetic insulators to ferromagnetic insulators at T_c. There is much interest in finding a structural change at T_c in the giant magnetoresistive manganites, since it is predicted to have a large effect on the resistive transition.[4] There is now evidence[35–38] for a decrease in structural disorder as the magnetoresistive manganites become ferromagnetic metals. $Gd_{0.67}Ca_{0.33}MnO_3$ shows the contrapositive: there is no discontinuity in the atomic disorder for a material which does not become metallic at T_c. This has also been noted in manganites with different dopant concentrations: $La_{0.88}Ca_{0.12}MnO_3$ (Ref. 35) and $La_{0.5}Ca_{0.5}MnO_3$.[38]

V. CONCLUSION

$Gd_{0.67}Ca_{0.33}MnO_3$ is ferrimagnetic with a compensation temperature of about 15 K due to the interaction and ordering of the Gd^{3+} moments. The qualitative features of the magnetic properties can be accounted for with a simple two sublattice (Gd and Mn) molecular field model. The large high-field susceptibility at low temperatures may indicate a canting of the magnetic sublattices. Contrary to the conclusion in Ref. 7 that there does not exist long-range magnetic order (only spin-glass magnetism) in the ferromagnetic-insulator region of the tolerance-factor phase diagram, $Gd_{0.67}Ca_{0.33}MnO_3$ shows definite long-range order and a compensation point which cannot be explained by spin-glass phenomena alone. The resistivity is consistent with small polaron conductivity over a broad temperature range, with a possible crossover to a different mechanism such as variable-range hopping at low temperatures. There is no noticeable change in the structure, as determined by XAFS, or conductivity at the ferrimagnetic transition. Recent theoretical and experimental work concludes that structural effects at T_c are associated with the metal-insulator transition and large magnetoresistance. Since $Gd_{0.67}Ca_{0.33}MnO_3$ is in the doping regime where a metal-insulator transition and large magnetoresistance are *not* observed at T_c, this work supports that conclusion, i.e., that a significant structural change is associated not with the ferromagnetic transition, but with the metal-insulator transition.

ACKNOWLEDGMENTS

We would like to thank Vlad Beffa, Sossina Haile, R. S. Feigelson, Roger Route, Daniel Worledge, Laurent Mieville, R. L. White, and Shan Wang for their help in this project. The work at Stanford was supported in part by the Air Force Office of Scientific Research and the Stanford Center for Materials Research under the NSF-MRL program. G.J.S. would like to acknowledge the support of the Hertz foundation.

[1] P. Shuk, L. Tichonova, and U. Guth, Solid State Ion. **68**, 177 (1994).
[2] C. Herring, in *Magnetism*, edited by G. T. Rado and H. Suhl (Academic, New York, 1964), Vol. V.
[3] G. J. Snyder, R. Hiskes, S. DiCarolis, M. R. Beasley, and T. H. Geballe, Phys. Rev. B **53**, 14 434 (1996).
[4] A. J. Millis, B. I. Shraiman, and R. Mueller, Phys. Rev. Lett. **77**, 175 (1996).
[5] P. Schiffer, A. P. Ramirez, W. Bao, and S.-W. Cheong, Phys. Rev. Lett. **75**, 3336 (1995).
[6] H. Y. Hwang, S.-W. Cheong, P. G. Radaelli, M. Marezio, and B. Batlogg, Phys. Rev. Lett. **75**, 914 (1995).
[7] J. M. DeTeresa, M. R. Ibarra, J. Garcia, J. Blasco, C. Ritter, P. A. Algarabel, C. Marquina, and A. delMoral, Phys. Rev. Lett. **76**, 3392 (1996).
[8] R. S. Feigelson, D. Gazit, D. K. Fork, and T. H. Geballe, Science **240**, 1642 (1988).
[9] C. A. Burrus and L. A. Coldren, Appl. Phys. Lett. **31**, 383 (1977).
[10] R. Hiskes, S. A. DiCarolis, J. Fouquet, Z. Lu, R. S. Feigelson, R. K. Route, F. Leplingard, and C. M. Foster, in Metal-Organic Chemical Vapor Deposition of Electronic Ceramics, edited by S. B. Desu, D. B. Beach, B. W. Wessels, and S. Gokoglu, MRS Symposia Proceedings No. 335 (Materials Research Society, Pittsburgh, 1994), p. 299.
[11] G. J. Snyder, Thesis, Stanford, 1997.
[12] R. M. White and T. H. Geballe, in *Solid State Physics*, edited by H. Ehrenreich, F. Seitz, and D. Turnbull (Academic, New York, 1979), Vol. 15.
[13] L. J. van der Pauw, Philips Tech. Rev. **20**, 220 (1958).
[14] T. M. Hayes and J. B. Boyce, in *Solid State Physics*, edited by H. Ehrenreich, F. Seitz and D. Turnbull (Academic, New York, 1982), Vol. 37, p. 173.
[15] J. B. Goodenough, in *Progress in Solid State Chemistry*, edited by H. Reiss (Pergamon, Oxford, 1971), Vol. 5, Chap. 4, pp. 145–400.
[16] D. C. Worledge, G. J. Snyder, R. Hiskes, S. DiCarolis, M. R. Beasley, and T. H. Geballe, J. Appl. Phys. **80**, 5158 (1996).
[17] N. F. Mott and E. A. Davis, *Electronic Processes in Non-Crystalline Materials* (Clarendon Press, Oxford, 1971).
[18] R. Pauthenet, J. Appl. Phys. **29**, 253 (1958).
[19] A. S. Yermolenko, Phys. Met. Metallogr. **50** (4), 57 (1980).
[20] H. Yoshizawa, H. Kawano, Y. Tomioka, and Y. Tokura, Phys. Rev. B **52**, 13 145 (1995).
[21] Z. Jirak, S. Krupicka, Z. Simsa, M. Dlouha, and S. Vratislav, J. Magn. Magn. Mater. **53**, 153 (1985).
[22] I. S. Jacobs, J. Phys. Chem. Solids **11**, 1 (1959).
[23] I. S. Jacobs, J. Phys. Chem. Solids **15**, 54 (1960).
[24] A. H. Morrish, *The Physical Principles of Magnetism* (Wiley, New York, 1965).
[25] J. J. Melero, F. Bartolome, J. Bartolome, and R. Burriel (unpublished).
[26] G. C. Xiong, Q. Li, H. L. Ju, S. N. Mao, L. Senapati, X. X. Xi, R. L. Greene, and T. Venkatesan, Appl. Phys. Lett. **66**, 1427 (1995).
[27] Z. Jirak, S. Krupicka, V. Nekvasil, E. Pollert, G. Villeneuve, and F. Zounova, J. Magn. Magn. Mater. **15–18**, 519 (1980).

[28] D. Emin and T. Holstein, Ann. Phys. **53**, 439 (1969).
[29] H. Taguchi, M. Nagao, and M. Shimada, J. Solid State Chem. **97**, 476 (1992).
[30] G. J. Snyder, R. Hiskes, S. DiCarolis, M. R. Beasley, and T. H. Geballe, Appl. Phys. Lett. **69**, 4254 (1996).
[31] H. Taguchi, M. Nagao, and M. Shimada, J. Solid State Chem. **82**, 8 (1989).
[32] B. I. Shklovskii and A. L. Efros, *Electronic Properties of Doped Semiconductors* (Springer-Verlag, Berlin, 1984).
[33] V. Ambegaokar, B. I. Halperin, and J. S. Langer, Phys. Rev. B **4**, 2612 (1971).
[34] J. M. D. Coey, M. Viret, and L. Ranno, Phys. Rev. Lett. **75**, 3910 (1995).
[35] S. J. L. Billinge, R. G. DiFrancesco, G. H. Kwei, J. J. Neumeier, and J. D. Thompson, Phys. Rev. Lett. **77**, 715 (1996).
[36] R. P. Sharma, G. C. Xiong, C. Kwon, R. Ramesh, and R. L. Greene, Phys. Rev. B **54**, 10 014 (1996).
[37] P. G. Radaelli, M. Marezio, H. Y. Hwang, S.-W. Cheong, and B. Batlogg, Phys. Rev. B **54**, 8992 (1996).
[38] C. H. Booth, F. Bridges, G. J. Snyder, and T. H. Geballe, Phys. Rev. B **54**, 15 606 (1996).